Inorganic Chemistry

ARTICLE

pubs.acs.org/IC

Structural, Magnetic, and Gas Adsorption Study of a Series of Partially Fluorinated Metal−Organic Frameworks (H*F*-MOFs)

Pradip Pachfule, Raja Das, Pankaj Poddar, and Rahul Banerjee*

Physical/Materials Chemistry Division, National Chemical Laboratory, Dr. Homi Bhabha Road, Pune, 411008, India

Supporting Information

ABSTRACT: Four new partially fluorinated metal organic frameworks (H*F*-MOFs) have been synthesized under different solvothermal conditions (H_2O or dimethylformamide (DMF)) from transition metal cations [Co^{2+} and Mn^{2+}], 3-methyl pyridine (3-mepy) and 4,4′-(hexafluoroisopropylidene) bis(benzoic acid) ($C_{17}H_{10}F_6O_4$, H_2hfbba), to determine the influence of reaction conditions on the formation of MOFs. This family of materials displays a striking degree of structural similarity depending on the solvent of synthesis. H*F*-MOFs synthesized from H_2O [Co-H*F*MOF-W, Co(hfbba)(3-mepy)(H_2O) and Mn-H*FMOF*-W, Mn(hfbba)(3-mepy)(H_2O)] contain three-dimensional connectivity whereas H*F*-MOFs synthesized from DMF Co-H*F*MOF-D, [Co_2(hfbba)$_2$(3-mepy)$_2$]·(DMF)$_3$ and Mn-H*F*MOF-D, [Mn_2(hfbba)$_2$(3-mepy)]·(H_2O) are two-dimensional in nature. Co-H*F*MOF-W and Mn-H*F*MOF-W are iso-structural polymeric materials. Thermal gravimetric analysis performed on as-synthesized H*F*-MOFs revealed that these compounds have high thermal stability (∼350 °C). The continuous decrease of the χT product with decreasing T for Co-H*F*MOF-D and Co-H*F*MOF-W respectively indicates the presence of antiferromagnetic exchange interaction between two Co^{2+} ($S = 3/2$) metal centers within a cluster.

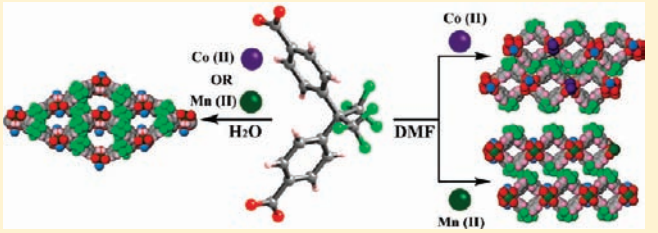

INTRODUCTION

Metal−organic frameworks (MOFs)[1] represent a new class of network solids that have great potential in specific applications like separation,[2] storage,[3] heterogeneous catalysis,[4] and controlled drug delivery.[5] Extensive research has been done on MOFs as these materials are good for storing hydrogen[6] and carbon dioxide.[7] The hydrogen and carbon dioxide storage capacity in MOFs can be enhanced in various ways, such as introducing open metal sites, increasing surface area and pore volume, functionalizing organic linkers, and utilizing catenation.[8] Yang et al.,[9] in this regard, have explored for the first time the possibility of synthesizing Fluorinated Metal Organic Frameworks (*F*MOFs) using perfluorinated polycarboxylate ligands with porous surfaces and exposed fluorine atoms for interesting H_2 storage properties. They have reported hysteretic 2-step, and one of the highest volumetric capacities for H_2 adsorption which later has been independently reviewed by Fischer and Wöll.[10] Later, Cheetham and co-workers[11a,b] and others[11c−f] also explored the interesting H_2 and CO_2 storage properties in partially fluorinated MOFs or mixed perfluorinated and nonfluorinated ligands. In all these reports researchers have agreed that MOFs with fluoro-lined or fluoro-coated channels are expected to possess enhanced affinity and selectivity toward gas adsorption compared to their nonfluorous counterparts.

Recently, we have synthesized several H*F*-MOFs with partially fluorinated dicarboxylic acids and transition metals in the presence of nitrogen containing coligands.[12] In the reaction of these fluorinated dicarboxylates, insertion of a coligand is required as often reaction of metal with these perfluorinated ligands, without these coligands, results in the precipitation of unreacted starting materials. It is noteworthy that MOF synthesis, in general, occurs in solvothermal media (water, organic solvents, ionic liquids), yet none of the synthetic details described in the literature explains the cause behind the solvent choice, despite it being an important parameter in the phase-pure synthesis of a desired phase.[13] As a result, it is still a challenge to predict the resulting structure of a MOF beforehand as its formation not only is influenced by the geometrical and electronic factors of metal ions and the organic links but also is dependent on other factors such as the rigidity or flexibility of the ligands, choice of solvent and solvent polarity, temperature, metal/ligand ratio, and pH.[14]

As a part of our ongoing investigation on the synthesis of different H*F*-MOFs, we studied the hydrothermal chemistry of 4,4′-(hexafluoroisopropylidene) bis(benzoic acid) (H_2hfbba) as a fluorinated ligand by incorporating it into the hybrid materials along with coligand 3-methyl pyridine (3-picoline) and Co^{2+} or Mn^{2+} as metal center.[15] To study the effect of solvent variation on the resulting H*F*-MOF framework, we used either DMF or H_2O as solvent of synthesis. These H*F*-MOFs formulated as [Co_2(hfbba)$_2$(3-mepy)$_2$]·(DMF)$_3$ (**Co-H*F*MOF-D**), [Co(hfbba)(3-mepy)(H_2O)] (**Co-H*F*MOF-W**), [Mn_2(hfbba)$_2$(3-mepy)]·(H_2O) (**Mn-H*F*MOF-D**), [Mn(hfbba)(3-mepy)(H_2O)] (**Mn-H*F*MOF-W**) display interesting two-dimensional (2-D, in DMF) and three-dimensional (3-D, in H_2O) structural features based on the solvent of synthesis (Scheme 1). Structures of these

Received: August 25, 2010
Published: March 25, 2011

Scheme 1. Synthetic Details of All the H*F*-MOFs Reported in This Paper

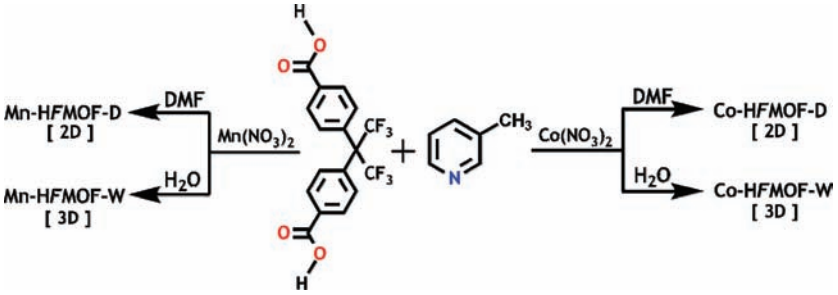

H*F*-MOFs have been determined by X-ray crystallography and further identified by IR spectroscopy, powder X-ray diffraction (PXRD), and thermogravimetric analysis (TGA). These H*F*-MOFs also show interesting H_2 and CO_2 uptake and magnetic properties based on their structural variation.

EXPERIMENTAL SECTION

General Procedures. All reagents and solvents for synthesis and analysis were commercially available and used as received. The Fourier transform (FT) IR spectra (KBr pellet) were taken on a Perkin Elmer FT-IR Spectrum (Nicolet) spectrometer. PXRD patterns were recorded on a Phillips PANalytical diffractometer for Cu Kα_1 radiation (λ = 1.5406 Å), with a scan speed of 2° min^{-1} and a step size of 0.02° in 2θ. TGA was carried out in the temperature range of 15−900 °C on a SDT Q600 TG-DTA analyzer under N_2 atmosphere at a heating rate of 10 °C min^{-1}. All low pressure gas adsorption experiments (up to 1 bar) were performed on a Quantachrome Quadrasorb automatic volumetric instrument. Direct current (DC) magnetization versus T curves were taken at a 500 Oe field in field cooled (FC) and zero field cooled (ZFC) modes with heating/cooling rate of 2 K per minute. Magnetizations versus field loops were taken in a field sweep from −50 kOe to +50 kOe at a rate of 75 Oe/sec. All the measurements were done using a Physical Property Measurement System (PPMS) from Quantum Design Inc., San Diego, U.S.A., equipped with a 7 T superconducting magnet and a vibrating sample magnetometer. The magnetic signal from the sample holder was negligible and did not affect our data accuracy.

Synthesis of [Co_2(hfbba)$_2$(3-mepy)$_2$]·(DMF)$_3$ (Co-H*F*MOF-D). A 0.5 mL portion of 3-methyl pyridine stock solution and 1.5 mL of H_2hfbba stock solution (0.20 M) were mixed in a 5 mL vial. To this solution was added 0.5 mL of $Co(NO_3)_2 \cdot 6H_2O$ stock solution (0.20 M). The vial was capped and heated to 85 °C for 96 h. The mother liquor was decanted, and the products were washed with DMF (15 mL) three times. Dark pink colored crystals of Co-H*F*MOF-D were collected by filtration and dried in air (10 min) [Yield: 52%, 0.0151 g depending on $Co(NO_3)_2 \cdot 6H_2O$]. ***FT-IR:*** (KBr 4000−450 cm^{-1}): 3393(m, br), 2935(w), 19441(w), 1628(m), 1406(s), 1172(s), 929(m), 780(m), 481(m) cm^{-1}.

Synthesis of [Co(hfbba)(3-mepy)(H_2O)] (Co-H*F*MOF-W). Hydrothermal reaction of $Co(NO_3)_2 \cdot 6H_2O$ (0.035, 0.12 mmol) with 0.5 mL of 3-methyl pyridine and excess H_2hfbba (0.196 g, 0.50 mmol) in a 25 mL acid-digestion bomb using deionized water (7 mL) at 85 °C for 96 h produced pink colored crystals of Co-H*F*MOF-W. Crystals were collected by filtration, washed with ethanol, and dried in air (10 min). [Yield: 42%, 0.0147 g depending on $Co(NO_3)_2 \cdot 6H_2O$]. ***FT-IR:*** (KBr 4000−450 cm^{-1}): 3203 (m, br), 3088(w), 2528(w), 1697(m), 1609(s), 1546(m), 1392(s), 1293(m), 1171(m), 930(w), 786(m), 725(m), 512(w) cm^{-1}.

Synthesis of [Mn_2(hfbba)$_2$(3-mepy)]·(H_2O) (Mn-H*F*MOF-D). A 0.5 mL portion of 3-methyl pyridine stock solution and 1.5 mL of H_2hfbba stock solution (0.20 M) were mixed in a 5 mL vial. To this solution was added 0.5 mL of $Mn(NO_3)_2 \cdot xH_2O$ stock solution (0.20 M). The vial was capped and heated to 85 °C for 96 h. The mother liquor was decanted, and the products were washed with DMF (15 mL) three times. Colorless crystals of Mn-H*F*MOF-D were collected by filtration and dried in air (10 min). [Yield: 47%, 0.0134 g depending on $Mn(NO_3)_2 \cdot xH_2O$]. ***FT-IR:*** (KBr 4000−450 cm^{-1}): 3225(m, br), 1965(m), 1624(m), 1550(s), 1390(s), 1242(s), 1171(m), 957(s), 784(s), 555 (w) cm^{-1}.

Synthesis of [Mn(hfbba)(3-mepy)(H_2O)] (Mn-H*F*MOF-W). Hydrothermal reaction of $Mn(NO_3)_2 \cdot xH_2O$ (0.035, 0.12 mmol) with 0.5 mL of 3-methyl pyridine and excess H_2hfbba (0.196 g, 0.50 mmol) in a 25 mL acid-digestion bomb using deionized water (7 mL) at 85 °C for 96 h produced colorless crystals of Mn-H*F*MOF-D. Crystals were collected by filtration, washed with ethanol, and dried in air (10 min). [Yield: 61%, 0.0213 g depending on $Mn(NO_3)_2 \cdot xH_2O$]. ***FT-IR:*** (KBr 4000−450 cm^{-1}): 3207 (m, br), 3090(w), 2528(w), 1697(m), 1610(s), 1547(m), 1390(s), 1292(m), 1248(s), 1171(m), 933(w), 785(m), 730(m), 514(w) cm^{-1}.

X-ray Crystallography. All single crystal data were collected on a Bruker SMART APEX three circle diffractometer equipped with a CCD area detector (Bruker Systems Inc., 1999a)[16] and operated at 1500 W power (50 kV, 30 mA) to generate Mo Kα radiation (λ = 0.71073 Å). The incident X-ray beam was focused and monochromated using Bruker Excalibur Gobel mirror optics. Crystals of the H*F*-MOFs reported in the paper were mounted on nylon CryoLoops (Hampton Research) with Paraton-N (Hampton Research). Data were integrated using Bruker SAINT software.[17] Data were subsequently corrected for absorption by the program SADABS.[18] The space group determinations and tests for merohedral twinning were carried out using XPREP.[19] In all cases, the highest possible space group was chosen. All structures were solved by direct methods and refined using the SHELXTL 97 software suite.[20] Atoms were located from iterative examination of difference F-maps following least-squares refinements of the earlier models. Hydrogen atoms were placed in calculated positions and included as riding atoms with isotropic displacement parameters 1.2−1.5 times U_{eq} of the attached C atoms. Data were collected at 298(2) K for all the H*F*-MOFs reported in this paper. All structures were examined using the Addsym subroutine of PLATON[21] to ensure that no additional symmetry could be applied to the models. All ellipsoids in ORTEP diagrams are displayed at the 50% probability level unless noted otherwise. The Supporting Information contains a detailed data collection strategy and crystallographic data for the four H*F*-MOFs reported in this paper. Crystal data and details of data collection, structure solution, and refinement are summarized in Table 1. Crystallographic data (excluding structure factors) for the structures reported in this paper have been deposited with the CCDC as deposition Nos. CCDC 788025−788028 (see also Table 1). Copies of the data can be obtained, free of charge, on application to the CCDC, 12 Union Road, Cambridge CB2 lEZ, U.K. (fax: + 44 (1223) 336 033; e-mail: deposit@ccdc.cam.ac.uk).

Table 1. Crystal Data and Structure Refinement for HF-MOFs Reported in This Paper

	Co-HFMOF-D	Co-HFMOF-W	Mn-HFMOF-D	Mn-HFMOF-W
empirical formula	$C_{28}H_{20}F_6N_4O_7$ Co	$C_{23}H_{17}F_6NO_5Co$	$C_{23}H_{16}F_6NO_{4.5}Mn$	$C_{23}H_{17}F_6NO_5Mn$
formula weight	696.65	560.31	547.31	556.32
crystal system	monoclinic	orthorhombic	monoclinic	orthorhombic
space group	$C2/c$	$Pna2_1$	$C2$	$Pna2_1$
unit cell dimensions	a = 26.957(19) Å	a = 26.194(13) Å	a = 28.086(8) Å	a = 26.406(8) Å,
	b = 11.025(8) Å	b = 10.524(5) Å	b = 7.583(2) Å	b = 10.626(3) Å,
	c = 24.602(15) Å	c = 8.243(4) Å	c = 12.109(3) Å	c = 8.473(3) Å
	β = 119.74(3)°		β = 105.461(5)°	
volume	6349(7)	2272.4(19)	2485.6(11)	2377.3(13)
Z	8	4	2	4
density (calculated)	1.458	1.638	1.463	1.554
reflections collected	5402	5254	4365	4182
independent reflections	4980	4653	2991	3773
data/restraints/parameters	5402/16/331	5254/2/332	4365/4/320	4182/2/334
goodness-of-fit on F^2	1.054	1.095	1.010	1.052
final R indices $[I > 2\sigma(I)]$	R_1 = 0.1297	R_1 = 0.0550	R_1 = 0.0682	R_1 = 0.0354
	wR_2 = 0.3308	wR_2 = 0.1133	wR_2 = 0.1675	wR_2 = 0.0913
R indices (all data)	R_1 = 0.1343	R_1 = 0.0641	R_1 = 0.0959	R_1 = 0.0405
	wR_2 = 0.3359	wR_2 = 0.1168	wR_2 = 0.1797	wR_2 = 0.0935
largest diff. peak and hole	0.163 and −0.959 e Å^{-3}	0.088 and −0.998 e Å^{-3}	0.100 and −0.361e Å^{-3}	0.055 and −0.326 e Å^{-3}

H_2 and CO_2 Adsorption Measurements. Hydrogen adsorption−desorption experiments were conducted at 77 K using a Quantachrome Quadrasorb automatic volumetric instrument. Ultrapure H_2 (99.95%) was purified further by using calcium aluminosilicate adsorbents to remove trace amounts of water and other impurities before introduction into the system. For measurements at 77 K, a standard low-temperature liquid nitrogen dewar vessel was used. CO_2 adsorption−desorption measurements were done at room temperature (298 K). Before gas adsorption measurements, the sample was activated at room temperature (for 24 h) and 100 °C (for 36 h) under ultrahigh vacuum (10^{-8} mbar) overnight. About 75 mg of samples were loaded for gas adsorption, and the weight of each sample was recorded before and after outgassing to confirm complete removal of all guest molecules including the coordinated H_2O in Co-HFMOF-W and Mn-HFMOF-W.

RESULTS AND DISCUSSION

Synthesis. We used 4,4′-(hexafluoroisopropylidene) bis-(benzoic acid) because (a) a twisted conformation of this ligand could lead to a possible helical architecture,[12a] (b) different deprotonated degrees of the ligands under different reaction conditions may result in variable coordination modes in the products, and (c) long and bent molecular structure of this primary building unit may lead to the formation of microporous coordination frameworks with channels. Influence of the solvent (DMF/H_2O) on the structure of these MOFs was reflected in their structure. Co-HFMOF-D and Mn-HFMOF-D, synthesized from DMF, contain 2-D connectivity whereas Co-HFMOF-W and Mn-HFMOF-W, synthesized from H_2O, are 3-D in nature.[22] It is noteworthy that our previous experience while synthesizing HF-MOFs from water resulted in zero or one-dimensional (1-D) connectivity, whereas the same from DMF created a 3-D structure. We will first discuss the crystal structure of HF-MOFs that have been synthesized in DMF and follow that by a discussion of the structures synthesized in H_2O.

DESCRIPTION OF CRYSTAL STRUCTURES

Crystal Structure of $[Co_2(hfbba)_2(3\text{-mepy})_2]\cdot(DMF)_3$ (Co-HFMOF-D). Crystal structure of Co-HFMOF-D contains two crystallographically independent Co^{2+} ions, two hfbba ligands, two 3-methyl pyridine ligands, and three lattice DMF molecules in its asymmetric unit (Figure 1a). Both Co^{2+} centers of Co-HF-MOF-D have almost the same coordination environments with a nearly ideal square-pyramidal sphere ($\tau \approx 0$)[23] enclosed by four hfbba ligands [Co−O distance ranges from 2.024(2) to 2.051(2) Å] and one 3-methyl pyridine ligand [Co−N = 2.051(3) Å]. The dicobalt paddlewheel SBU (secondary building unit)[24] for Co-HFMOF-D with the Co···Co distance of 2.746(1)Å is shown in Figure 1a, expanded to show the four hfbba ligands, each coordinated to a dicobalt paddlewheel unit via one of their carboxylate groups. The second carboxylate group of each hfbba ligand coordinates to another paddlewheel unit, generating the extended corrugated 2-D layered structure (Figure 1b). In Co-HFMOF-D, 3-methyl pyridine ligands occupy the axial positions of dicobalt paddlewheel, blocking the pores. By joining only Co^{2+} centers with ligand atoms, topological simplification of Co-HFMOF-D shows the formation of square shaped pores and the mode of attachment of ligands with the metal center as shown in Figure 1c. In Co-HFMOF-D, the sheets stack along b axis affording square-shaped channels from the sheet cavities that run through the gross structure (Figure 1d) creating a square grid topology. The distance between equivalent atoms in between neighboring sheets is approximately 3.5 Å. The $-CF_3$ groups of H_2hfbba ligands are directed to the outside of the larger square channels while one DMF molecule is sitting inside the pore and two are arranged in the interlayer region respectively. The pore diameter for Co-HFMOF-D is ∼3.106 Å across, based on largest sphere that could fit into the pore and also remain in contact with the van der Waals surface.[25] The $-CF_3$ groups of one channel in Co-HFMOF-D are located in between the edges of the square shaped channel with a minimal interlayer void (Figure 1d).

dx.doi.org/10.1021/ic1017246 |Inorg. Chem. 2011, 50, 3855–3865

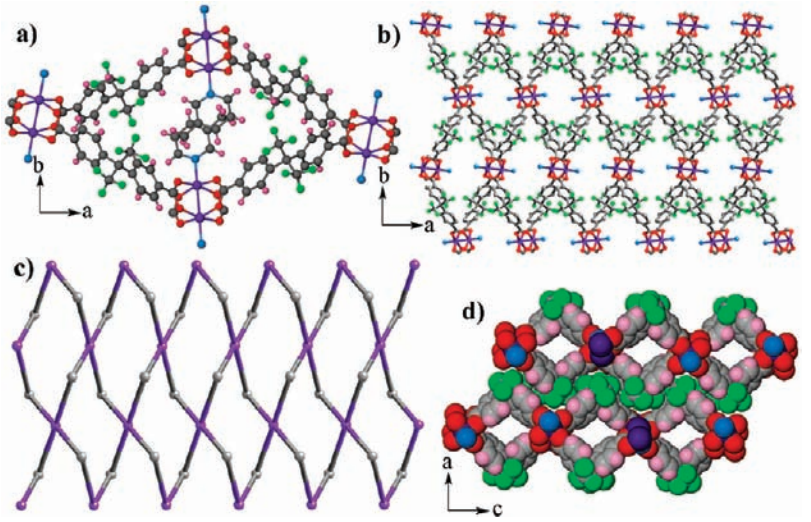

Figure 1. Crystal structure of **Co-H*F*MOF-D**. (a) Ball and Stick representation of the SBU showing the paddle-wheel motif of Co^{2+}. Two 3-methyl-pyridine ligands occupy the axial positions. (b) 2-D coordination layer in Co-H*F*MOF-D with Co^{2+} paddle-wheel binuclear nodes (view down *c* axis). (c) Topological simplification of Co-H*F*MOF-D, by joining only Co^{2+} centers (magenta) with carbon atoms of isopropyl group (black). (d) Coordination layer in Co-H*F*MOF-D (view down *b* axis) showing the 3.106 Å channels. Hydrogen atoms, guest molecules, and 3-methyl-pyridines are omitted for clarity. Color code: Co (magenta), N (blue), O (red), C (black), F (green).

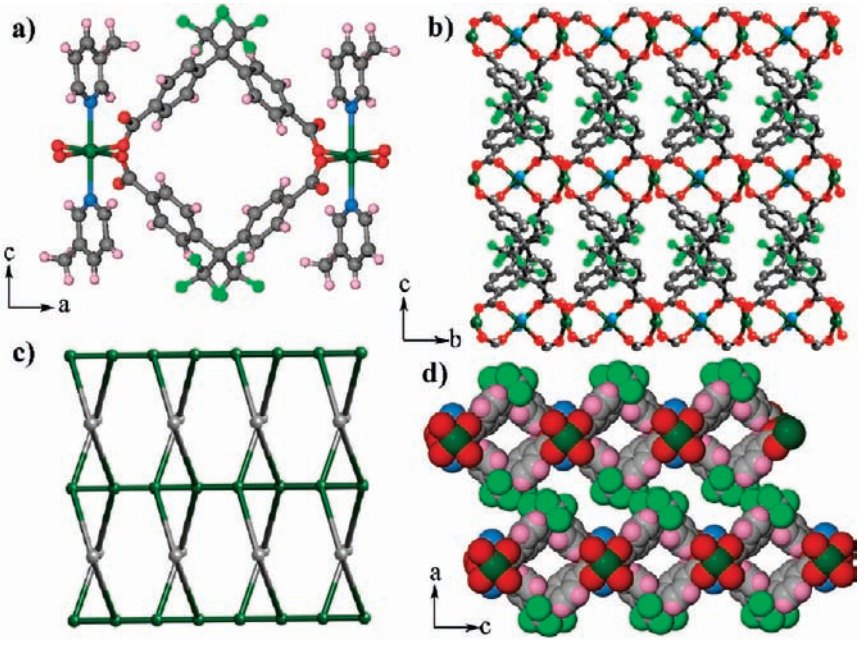

Figure 2. Crystal structure of **Mn-H*F*MOF-D**. (a) Ball and Stick representation of the SBU showing the binuclear $M_2N_2(\mu_2\text{-}CO_2)_2$ unit. (b) 2-D coordination layer in Mn-H*F*MOF-D with each hfbba ligand is connected to two Mn^{2+} metal centers (view down *a* axis). (c) Zigzag network topology of Mn-H*F*MOF-D, by joining only Mn^{2+} centers (green) with carbon atoms of isopropyl group (black). (d) Space fill Mn-H*F*MOF-D (view down *b* axis) showing the 3.002 Å channels; note the large interlayer void compared to Co-H*F*MOF-D. Hydrogen atoms, guest molecules, and 3-methyl-pyridines are omitted for clarity. Color code: Mn (green), N (blue), O (red), C (black), F (light green).

The 2-D parallel interpenetrating network is reinforced by the existence of other noncovalent interactions like C−H···F hydrogen bonds (*D*, 3.327 Å; *d*, 2.774 Å; *θ*, 117.32°).[26]

Crystal Structure of $[Mn_2(hfbba)_2(3\text{-mepy})]\cdot(H_2O)$ (Mn-H*F*MOF-D). In the 2-D structure of Mn-H*F*MOF-D, the asymmetric unit is composed of one Mn^{2+} ion, one hffbba ligand, one 3-methyl pyridine ligand, and one lattice H_2O molecule. Two different types of co-ordination environments around Mn^{2+} are found in Mn-H*F*MOF-D. As a result there are two types of SBUs in the binuclear Mn-H*F*MOF-D unit (Figure 2a). Among these SBUs, one is in octahedral co-ordination geometry as four hfbba ligands [Mn_{oct}−O distance ranges from 2.158 (3) to 2.185 (2) Å] and two 3-methyl pyridine ligands [Mn−N = 2.266 (3) Å] are coordinated. Another SBU is in the square planar co-ordination sphere where only four hfbba ligands [Mn −O distance ranges from 2.113 (3) to 2.154 (2) Å and O−Mn−O angle ranges from

dx.doi.org/10.1021/ic1017246 |*Inorg. Chem.* 2011, 50, 3855–3865

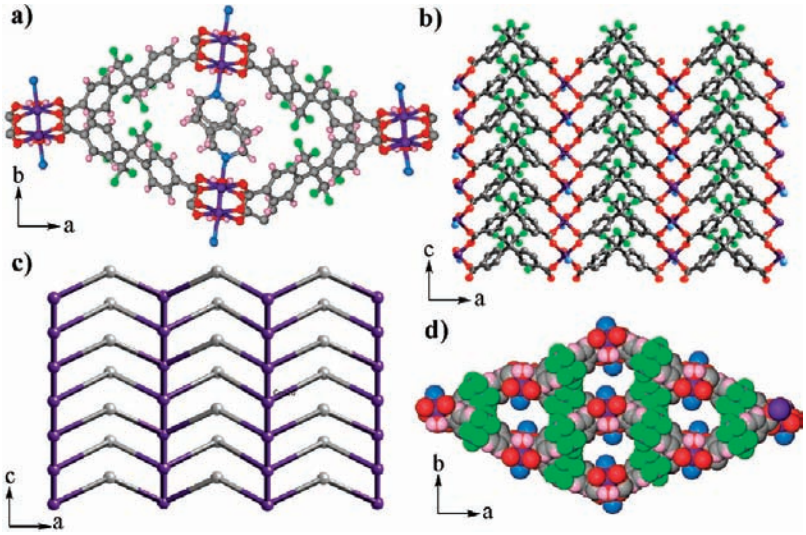

Figure 3. Crystal structure of **Co-HFMOF-W/Mn-HFMOF-W**. (a) Ball and stick representation of the SBU of Co-HFMOF-W showing the coordination environment around the metal. (b) Coordinated hfbba ligands form the zigzag type structure along the crystallographic *ac* plane. (c) Zigzag network topology of M-HFMOF-D, by joining only M^{+2} centers (magenta) with carbon atoms of isopropyl group (black). (d) Space filling model along crystallographic *ab* plane shows the formation of a 1-D channel assembling these square shaped pores. Hydrogen atoms, guest molecules, and 3-methyl-pyridines are omitted for clarity. Color code: M (magenta), N (blue), O (red), C (black), F (light green).

89.42° to 95.09°] are attached to the metal center. In this structure, these octahedral and square planar metal centers are arranged alternatively along the crystallographic *b* axis (Figure 2b). The crystal structure of Mn-HFMOF-D adopts a 2-D arrangement as the co-ordination of Mn^{2+}—hfbba—Mn^{2+} propagates along the *c* axis and simultaneously the Mn—CO_2—Mn propagates along the *b* axis. Since the octahedral Mn^{2+} sites are blocked by 3-methyl pyridine, which is a monodentate ligand, the crystal structure fails to propagate along the crystallographic *a* axis. In the crystal structure of Mn-HFMOF-D, each hfbba ligand is connected to two Mn^{2+} metal centers, that is, octahedral and square planar respectively through a zigzag fashion as shown in Figure 2b. By joining only Mn^{2+} centers with ligand atoms, the topological simplification of Mn-HFMOF-D shows the formation of a zigzag network and the mode of attachment of ligands with the metal center (Figure 2c). In the structure of Mn-HFMOF-D, the propagation of accessible square shaped pores of about 3.0 Å pore diameter is along the *b* axis in which lattice water molecules are sitting inside. Here $-CF_3$ groups are protruding outside the adjacent channels within interlayers which are spaced at 2.847 Å, in zigzag manner (Figure 2d). Unlike Co-HFMOF-D, $-CF_3$ groups of one channel in Mn-HFMOF-D are located on top of the square shaped channel edges with a significant interlayer void. The 2-D parallel interpenetrating network is reinforced by the existence of other noncovalent interactions like C—H···F hydrogen bonds (*D*, 3.302 Å; *d*, 2.530 Å; *θ*, 140.52°).[26]

Crystal Structures of [Mn(hfbba)(3-mepy)(H_2O)] (Mn-HFMOF-W) and [Co(hfbba)(3-mepy)(H_2O)] (Co-HFMOF-W). Three dimensional Mn-HFMOF-W and Co-HFMOF-W have been synthesized from H_2O, using hydrothermal conditions in an acid digestion bomb at 120 °C. Mn-HFMOF-W and Co-HFMOF-W are iso-structural containing Mn^{2+} and Co^{2+} metal centers (see the unit cell dimensions in Table 1) in the orthorhombic $Pna2_1$ space group. The asymmetric unit of Mn-HFMOF-W and Co-HFMOF-W contains one crystallographically independent Mn^{2+}/Co^{2+} ion, one hfbba ligand, one 3-methyl pyridine ligand, and one coordinated H_2O molecule. Each octahedral Mn^{2+}/Co^{2+} ion is surrounded by four oxygens from hfbba ligands [M—O distance ranges from 2.071 (2) to 2.212 (2) Å], one oxygen from H_2O [M—O distance =2.169-(3)—2.224(2) Å], and one nitrogen from 3-methyl pyridine ligand [M—N distance = 2.124—2.248 Å]. In Mn-HFMOF-W and Co-HFMOF-W, the metal—metal distance is 4.494 Å to 4.616 Å, which are connected through the COO^- group of hfbba ligands. In the SBU of Mn-HFMOF-W and Co-HFMOF-W, on the adjacent metal center 3-methyl pyridine ligands are coordinated above and below positions alternatively (Figure 3a). The coordinated water molecule is coordinated on the opposite side of 3-methyl pyridine ligand. Four hfbba ligands are coordinated to adjacent metal centers from one carboxyl group which extends further joining to the next SBU. In the structure of Mn-HFMOF-W and Co-HFMOF-W, alternatively joined 3-methyl pyridine ligands are interdigited in the pores by blocking them through the *ab* plane. In these structures, each hfbba ligand coordinates with two adjacent metal centers through one of its carboxyl groups, which extends further forming the hexagonal pores along with interpenetration of 3-methyl pyridine and coordinated water molecules inside. Coordinated hfbba ligands form the zigzag type structure along the crystallographic *ac* plane (Figure 3b). By joining only the Co^{2+}/Mn^{2+} centers with ligand atoms, the topological simplification of Mn-HFMOF-W and Co-HFMOF-W shows the formation of a zigzag network and the mode of attachment of ligands with metal center as shown in Figure 3c. The V shaped hfbba ligand when coordinating with the metals gives the square shaped pores. Space filling model of these MOFs along crystallographic *ab* plane shows the formation of a 1-D channel assembling these square shaped pores (Figure 3d).

We have synthesized four new polymeric frameworks Co-HFMOF-D, Co-HFMOF-W, Mn-HFMOF-D, and Mn-HFMOF-W as shown in Scheme 1, which forms 2-D and 3-D networks with diverse architectures depending on the solvent of synthesis. We expected that the insertion of additional 3-picoline ligand in the synthesis media should have a crucial effect, as they induces the Π—Π stacking interactions affecting the dimensionality of

dx.doi.org/10.1021/ic1017246 |*Inorg. Chem.* 2011, 50, 3855–3865

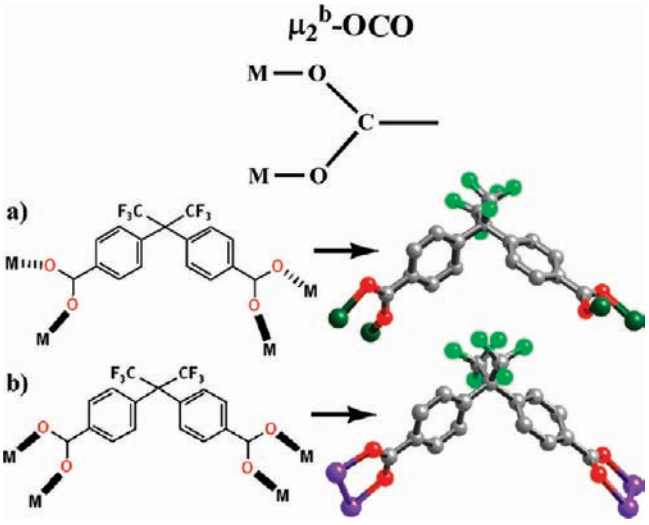

Figure 4. (a) μ_2^b−OCO bridging mode observed in **Co-H*F*MOF-W**, **Mn-H*F*MOF-W**, and **Mn-H*F*MOF-D**. (b) μ_2^b−OCO bridging mode observed in **Co-H*F*MOF-D**.

the resulting polymeric framework, and therefore its square grid topology. In all the structures 3-picoline occupies the axial position of the $M_2N_2(\mu_2\text{-}CO_2)_2$ or $M_2N_1O_1(\mu_2\text{-}CO_2)_2$ the co-ordination sphere (Figure 4). Bimetallic clusters formed by co-ordination of metal centers with carboxylate groups play an important role in the determination of the architecture of the resultant framework. In the H*F*-MOFs reported in this paper, the co-ordination mode is μ_2^b−OCO, that is, both the carboxylate oxygen atoms are involved in the co-ordination with two M^{+2} atoms in monodentate fashion (See Scheme 1 in Supporting Information for a detailed representation of the connectivity of $hfbba^{2-}$). Although the co-ordination mode is same in all H*F*-MOFs, their dimensionality, SBU, and resultant frameworks are totally different from each other. It seems that the solvent of synthesis and the conditions for reaction are affecting the network structures. Co-H*F*MOF-D and Mn-H*F*MOF-D synthesized from DMF have the 2-D structure, whereas Co-H*F*MOF-W [flack parameter: 0.01(2)] and Mn-H*F*MOF-W [flack parameter: 0.04-(2)][27] synthesized from H_2O have the isostructural 3-D architecture with an octahedral SBU in the same $Pna2_1$ space group as shown in Figure 5. The adoption of a noncentrosymmetric space group and 2_1 screw axis by these two H*F*-MOFs could be attributed to the bent nature of the hfbba link.[28] But Co-H*F*MOF-D and Mn-H*F*MOF-D synthesized from DMF have different structures (Co-H*F*MOF-D, octahedral SBU with paddlewheel; Mn-H*F*MOF-D, octahedral and square planar SBU in same structure) with different space groups ($C2/c$ in Co-H*F*MOF-D and $C2$ in Mn-H*F*MOF-D). Although combination of $hfbba^{2-}$ with M^{+2} can produce 10 possible bridging modes of $hfbba^{2-}$, we observe only one co-ordination mode (μ_2^b−OCO) along this series (Figure 4), even we changed solvent and synthetic conditions. Tetradentate bridging mode of $hfbba^{2-}$ results in the formation of bimetallic tetracarboxylate clusters in all the H*F*-MOFs, where apical positions are occupied either by 3-methyl pyridine or coordinated H_2O molecules (Figure 5). Within these H*F*-MOFs, Co-H*F*MOF-D and Mn-H*F*MOF-D show formation of 2-fold parallel 2-D→2-D interpenetration with a 1-D channel through the crystallographic *ac* plane (Figures 1d and 2d). Co-H*F*MOF-W and Mn-H*F*MOF-W on the other hand

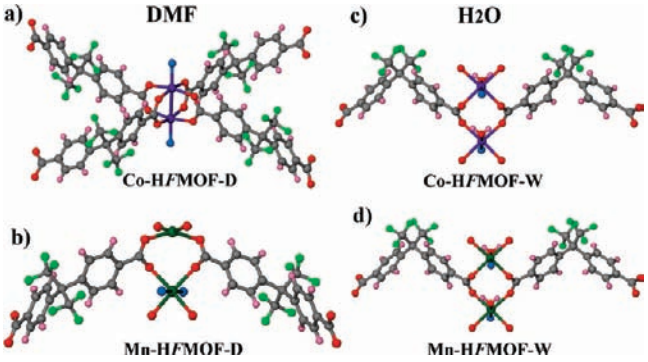

Figure 5. Different types of SBUs observed in all the H*F*-MOFs reported in the paper.

show formation of a 3-D framework with interdigited 3-methyl pyridine molecules (Figures 3a and 3d). Also, in these two H*F*-MOFs open metal sites can be observed as they contain the coordinated H_2O molecules which could be removed by strong evacuation.

Thermal Stability, PXRD Analysis. To examine the architectural and thermal stability of H*F*-MOFs reported in this paper, we prepared them at the gram scale to allow detailed investigation of the aforementioned properties. TGA performed on the as-synthesized Co-H*F*MOF-D, Co-H*F*MOF-W, Mn-H*F*MOF-D, and Mn-H*F*MOF-W revealed that these compounds have high thermal stability (see Section S3 in the Supporting Information for all data and interpretations regarding guest mobility and thermal stability of these H*F*-MOFs). The TGA trace for Co-H*F*MOF-D showed a gradual weight-loss step of ∼13.5% (15−200 °C), corresponding to escape of all DMF in the pores (3 DMF; calcd. ∼14%) followed by a sharp weight loss (200−450 °C) probably because of the decomposition of the coordinated 3-methyl pyridine molecules before decomposition of the framework. The TGA of Mn-H*F*MOF-D and Mn-H*F*MOF-W shows the sharp weight loss of ∼4.5% (15−100 °C) corresponding to escape of all H_2O molecules in pores (1 H_2O; calcd. ∼3.5% for Mn-H*F*MOF-W and ∼2.7% for Mn-H*F*MOF-D) followed by a plateau before a sharp weight loss (200−300 °C) probably because of the decomposition of the coordinated 3-methyl pyridine molecules. After 300 °C, the framework decomposes completely giving a 40% residue. The TGA of Co-H*F*MOF-W shows a gradual weight loss step of ∼11.5% (15−125 °C) corresponding to the loss of coordinated and framework water molecules (1 H_2O; calcd. ∼4.5%) followed by the decomposition of the framework probably because of decomposition of 3-methyl pyridine molecules and escape of coordinated H_2O molecules.

To confirm the phase purity of the bulk materials, PXRD experiments were carried out on all complexes. The PXRD of experimental and computer-simulated patterns of all of them are shown in the Supporting Information (Figure S1 to S4 in ESI). As shown in the figures, all major peaks of the experimental PXRD patterns of compounds Co-H*F*MOF-D, Co-H*F*MOF-W, Mn-H*F*MOF-D, and Mn-H*F*MOF-W match quite well with that of simulated PXRDs, indicating their reasonable crystalline phase purity. The experimental pattern of Co-H*F*MOF-D has a few diffraction lines that are unindexed and some that are slightly broadened in comparison with those simulated patterns. This is probably due to the loss of DMF molecules from the lattice because of grinding during the analysis.

dx.doi.org/10.1021/ic1017246 |*Inorg. Chem.* 2011, 50, 3855–3865

Gas Adsorption Experiments. The crystal structures of these H*F*-MOFs confirmed that all of them have small pores of 3−4 Å in diameter, so we concentrated on the gas adsorption studies of these H*F*-MOFs. Recently researchers investigated that open metal sites and solvent free frameworks are more useful for gas adsorption. So as-synthesized samples of Co-H*F*MOF-D, Co-H*F*MOF-W, Mn-H*F*MOF-D, and Mn-H*F*MOF-W were immersed in dry chloroform at ambient temperature for 72 h, evacuated at ambient temperature for 24 h, then at an elevated temperature 100 °C for 36 h under ultrahigh vacuum (10^{-8} mbar) overnight, to create a solvent free framework. Samples thus obtained were optimally evacuated, as evidenced by their well-maintained PXRD patterns and the long plateau (ambient temperature to 350 °C) in their TGA traces.

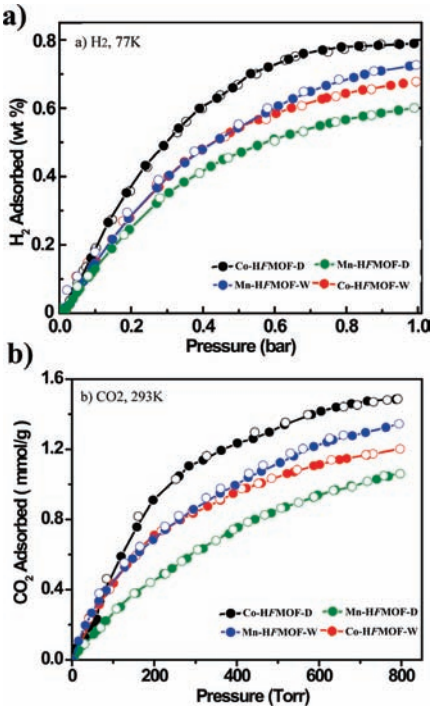

Figure 6. H_2 (77 K) and CO_2 (298 K) isotherm of the H*F*-MOFs reported in the paper. Filled and open symbols represent adsorption and desorption branches, respectively.

All of these four H*F*-MOFs are nonporous to N_2 as they have a lesser aperture size than the kinetic diameter of N_2 (3.6 Å); however, these H*F*-MOFs are able to take the H_2 (2.89 Å) and CO_2 (3.4 Å) as they have a lesser kinetic diameter. Furthermore, the low kinetic energy of the N_2 molecules at 77 K result in N_2 molecules being unable to effectively enter small pores.[29] All these H*F*-MOFs show reversible type I H_2 and CO_2 adsorption isotherms at 77 K and 298 K, respectively. Co-H*F*MOF-D showed highest reversible type I H_2 and CO_2 adsorption in this series, that is, 0.78 wt % and 1.48 mmol/g as pressure approaches to 1 atm as shown in Figure 6. Iso-structural Co-H*F*MOF-W and Mn-H*F*MOF-W show nearly the same 0.67 and 0.72 wt % of H_2 uptake, and 1.20 and 1.34 mmol/g of CO_2 adsorption. Mn-H*F*MOF-D shows the lowest H_2 (0.60 wt %) and CO_2 (1.06 mmol/g) adsorption. This result is well anticipated as Co-H*F*MOF-D contains the robust paddle-wheel Co(II) motif with 3-methyl pyridine pointing outward of the pore. As a result the pores are accessible to gases. On the other hand Co-H*F*MOF-W and Mn-H*F*MOF-W have 3-methyl pyridine molecules blocking the pore. Although H_2 adsorption for these H*F*-MOFs are somewhat moderate, they still are comparable with the H_2 adsorption of the highest capacity zeolites, some carbon materials, and some other H*F*-MOFs reported in the literature[11a−f,30] (see Table 2 for detailed comparison of H_2 and CO_2 uptake of *F*-MOFs reported so far). It is noteworthy that these materials show much higher volumetric H_2 and CO_2 uptake because of their high material density (see section S4 in the Supporting Information for a detailed description of volumetric H_2 and CO_2 uptake of the H*F*-MOFs reported).

Magnetic Properties. Magnetic interaction arises from the effective coupling of the paramagnetic centers through bridging groups of the crystal framework. Here we have shown how magnetic interaction changes with the distance between paramagnetic metal centers. The temperature dependence of the magnetic susceptibility (χ) and the effective magnetic moment (μ_{eff}) for Co-H*F*MOF-D and Co-H*F*MOF-W is shown in Figure 7, panels a and b. At 300 K, μ_{eff} values were calculated as

Table 2. Hydrogen and Carbon Dioxide Uptake Data of H*F*-MOFs Reported so Far

name of MOF[b]	H_2[a] wt %	CO_2 mmol/g
$[Zn_2(tfbdc)_2\ (dabco)]$[11f]	1.78 wt %	
$[Co_3(hfbba)_6\ (phen)_2]$[12a]	0.90 wt %	
$[Cu_2(hfbba)_2\ (3\text{-mepy})_2]\cdot(DMF)_2\ (3\text{-mepy})$[12b]	0.58 wt %	
$[Zn_5(triazole)_6\ (tfbdc)_2(H_2O)_2]\cdot(4H_2O)$[11a]	0.43 wt %	
$[Cu(hfipbb)(H_2hfipbb)_{0.5}]$[11c]	0.23 wt %	
$[Co_2(hfbba)_2(3\text{-mepy})_2]\cdot(DMF)_3$ (**Co-H*F*MOF-D**)	0.78 wt %	1.48 mmol/g [298 K]
$[Mn(hfbba)(3\text{-mepy})(H_2O)]$ (**Mn-H*F*MOF-W**)	0.72 wt %	1.34 mmol/g [298 K]
$[Co(hfbba)(3\text{-mepy})(H_2O)]$ (**Co-H*F*MOF-W**)	0.67 wt %	1.20 mmol/g [298 K]
$[Mn_2(hfbba)_2(3\text{-mepy})]\cdot(H_2O)$ (**Mn-H*F*MOF-D**)	0.60 wt %	1.06 mmol/g [298 K]
$[Zn_2(hfipbb)_2\ (bpdab)]\cdot 2DMF$[11d]	0.87 wt % [20 atm]	2.67 mmol/g [195 K]
$[Cd_2(hfipbb)_2\ (DMF)_2]\cdot 2DMF$[11d]	0.57 wt % [20 atm]	1.83 mmol/g [195 K]
$[Zn_2(hfbba)_{1.5}]\cdot(DMF)\cdot 2(H_2O)$[11e]		1.04 mmol/g [293 K]
$[Cu(hfipbb)(H_2hfipbb)_{0.5}]$[11c]	1.1 wt % [48 atm]	
$[Ag_2\ (Ag_4\text{-}Tz_6)]$[9a]	2.33 wt % [64 atm]	

[a] Here it should be noted that wherever pressure and temperature are not mentioned, there the pressure is 1 atm and the temperature is 77 K. [b] tfbdc = Tetrafluoroterephthalic acid, dabco = 1,4-diazabicyclo[2.2.2]octane, hfbba = 4,4′-(Hexafluoroisopropylidene) bis(benzoic acid), phen = 1,10-phenanthroline, 3-mepy = 3-methyl pyridine, triazole = 1,2,4-triazole, Tz = 3,5-bis(trifluoromethyl)-1,2,4-triazole.

dx.doi.org/10.1021/ic1017246 |*Inorg. Chem.* 2011, 50, 3855–3865

5.5 and 4.4 μ_B for Co-H*F*MOF-D and Co-H*F*MOF-W, respectively, which are appreciably lower than the theoretical value of 7.7 μ_B for two Co^{2+} ions in an octahedral crystal field environment with 6 uncoupled spins. It can be noted from Figure 7, panels a and b, that the temperature dependent decreasing trend of μ_B is not the same for Co-H*F*MOF-D and Co-H*F*MOF-W. Moreover, the χT is also larger for Co-H*F*MOF-D than Co-H*F*MOF-W for the same number of Co^{2+} spins per molecular cluster unit. The reason could be the presence of intercluster coupling which is possible in the Co-H*F*MOF-D because of a relatively smaller intercluster Co^{2+} center distance (Co−Co distance = 2.746 Å). This also indicates the presence of short-range magnetic interactions. The continuous decrease of the χT product with decreasing T from room temperature values of 3.8 and 2.4 emu K/mol Oe to the lowest measured values of 0.8 and 0.6 emu K/mol Oe for Co-H*F*MOF-D and Co-H*F*MOF-W, respectively, indicates the presence of antiferromagnetic exchange interaction between the two Co^{2+} (S = 3/2) metal centers within a cluster.[31] At 5 K, a magnetic moment of 1.3 and 1.15 μ_B per Co^{2+} center is observed for Co-H*F*MOF-D and Co-H*F*MOF-W, respectively. These values are less than the spin only values for one unpaired electron (1.73 μ_B) for Co^{2+}. The field dependence of the magnetization at 5 K for Co-H*F*MOF-D and Co-H*F*MOF-W is shown in Figure 7c. In the case of Co-H*F*MOF-D we observed nonlinearity in the curve, but in Co-H*F*MOF-W, it is close to linear (or nonlinearity is quite small). The presence of nonlinearity and coercivity of 35 Oe in the magnetization versus field shows the presence of short-range interactions at low temperature in Co-H*F*MOF-D, which could be due to the short inter Co^{2+} ion interaction.

The Curie−Weiss fit of the inverse molar susceptibility χ^{-1} in the temperature regime 165−350 K yields θ = −278 and −55 K for Co-H*F*MOF-D and Co-H*F*MOF-W, respectively. The negative sign of the Weiss constant further suggests the presence of antiferromagnetic interaction between near neighbors, although the anisotropy of the octahedral Co^{2+} will also contribute to these values.[32] The lower value of the Weiss constant for Co-H*F*MOF-W than for Co-H*F*MOF-D can be attributed to a larger inter Co^{2+} ion distance in Co-H*F*MOF-W than in Co-H*F*MOF-D which reduces the inter cluster magnetic interaction as indicated above. At temperatures below 100 K, in the cases of Co-H*F*MOF-D the inverse molar susceptibility deviates from a linear segment showing the characteristic of an antiferromagnetic system because of short-range interaction only. The straight line fit of the inverse molar susceptibility χ^{-1} in this temperature regime in both the structures yields a Weiss constant θ value near to 0 K. This magnetic behavior gives a picture where the spins come to a halt because of spin frustration while aligning in an antiparallel fashion with decreasing thermal motion. We did not observe any divergence between the zero-field-cooled (ZFC) and field-cooled (FC) data in both the samples.

The temperature dependence of magnetic susceptibility and effective magnetic moment for Mn-H*F*MOF-D and Mn-H*F*MOF-W is

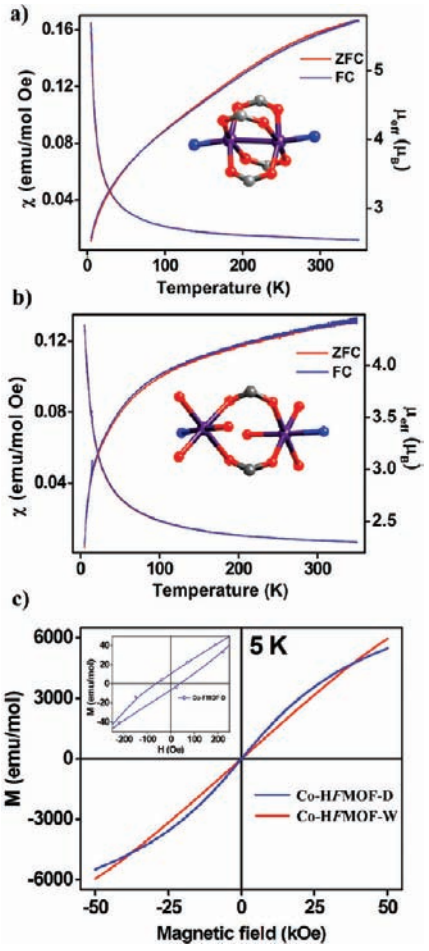

Figure 7. Temperature dependence of the magnetic susceptibility χ (left axis), the effective magnetic moment μ_{eff} (right axis) for (a) **Co-H*F*MOF-D** and (b) **Co-H*F*MOF-W**. Insets show ball and stick representation of the SBU of respective H*F*-MOFs showing the distance between two neighboring Co^{2+} atoms as 2.746 Å and 4.494 Å in **Co-H*F*MOF-D** and **Co-H*F*MOF-W**, respectively. (c) Field dependence of the magnetization for **Co-H*F*MOF-D** and **Co-H*F*MOF-W** at 5 K. Inset shows the opening of the hysteresis loop at 5 K for **Co-H*F*MOF-D**.

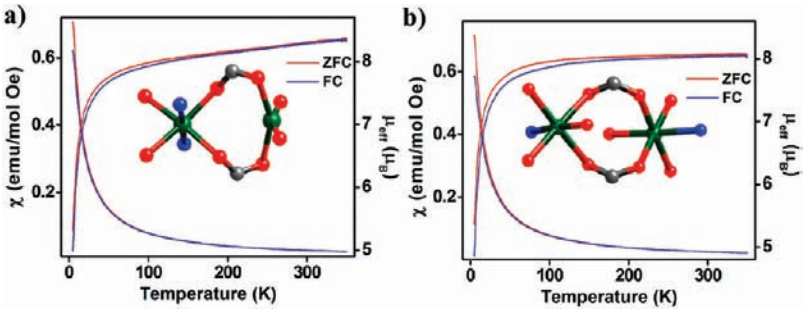

Figure 8. Temperature dependence of the magnetic susceptibility χ (left axis), the effective magnetic moment μ_{eff} (right axis) for (a) **Mn-H*F*MOF-D** and (b) **Mn-H*F*MOF-W**. Insets show ball and stick representation of the SBU of respective H*F*-MOFs showing the distance between two neighboring Mn^{2+} atoms, 3.732 Å and 4.616 Å, in **Mn-H*F*MOF-D** and **Mn-H*F*MOF-W**, respectively.

dx.doi.org/10.1021/ic1017246 |*Inorg. Chem.* 2011, 50, 3855–3865

shown in Figure 8. At 300 K, the effective magnetic moment of 8.3 and 8.0 μ_B for Mn-H*F*MOF-D and Mn-H*F*MOF-W respectively is once again appreciably lower than the theoretical value of 11.8 μ_B for two Mn^{2+} ions with 10 uncoupled spins. At 5 K, a magnetic moment of 2.55 and 2.5 μ_B per Mn^{2+} center is observed, a value slightly higher than the spin only value for one unpaired electron (1.73 μ_B). The extrapolation of the inverse molar susceptibility χ^{-1} in the temperature region (175−350 K) yields $\theta = -30$ K for Mn-H*F*MOF-D. The inverse molar susceptibility χ^{-1} for Mn-H*F*MOF-W shows the paramagnetic nature in the whole measured temperature range with a Weiss constant θ value near 0 K. As in the case of Co-H*F*MOF-W, there is no long-range magnetic ordering in the measured temperature region in Mn-H*F*MOF-D and Mn-H*F*MOF-W. The degree of spin frustration, *f*, in Mn-H*F*MOF-D is higher than 10, indicating strong frustration, but there is no spin frustration in Mn-H*F*MOF-W, since magnetic ordering is a cooperative effect which is determined by the magnetic coupling between paramagnetic centers through the bridging ligands. The framework structure gives the advantage of tailoring the magnetic property of the MOF by changing the paramagnetic metal center to center distance by changing the ligand, whereas in case of inorganic molecules this cannot be done.[28] In MOFs we can have designer's materials according to the required property.

CONCLUSION

A new series of partially fluorinated MOFs has been synthesized solvothermally, using bent ligand $hfbba^{2-}$ and divalent metal ions Co^{2+} and Mn^{2+}, along with terminal ligand 3-methyl pyridine. The bridging tetradentate mode of $hfbba^{2-}$ produces the bimetallic tetracarboxylate clusters in the all H*F*-MOFs. Co-H*F*MOF-D and Mn-H*F*MOF-D, synthesized from DMF, show formation of 2-fold parallel 2-D→2-D interpenetration with a 1-D channel whereas Co-H*F*MOF-W and Mn-H*F*MOF-W, synthesized from H_2O, show formation of a 3-D framework with interdigited 3-methyl pyridine molecules in pores. These results show that other factors like the solvent of synthesis, pH, and reaction temperature also play an important role on the adoption of the resulting MOF structure. In is noteworthy that previous work on partially fluorinated MOFs and an explicit comparison with nonfluorinated analogues imparted a disadvantage for fluorination. On the other hand, our results suggest that perfluorination is advantageous, which reinforces arguments made by Yang et al. and Cheetham and co-workers. All the H*F*-MOFs along this series shows comparable H_2 and CO_2 adsorption with other reported F-MOFs, and it is hard to prove or speculate on the adsorption data for the closest nonfluorinated MOF analogues of the MOFs we have reported in the paper. In our opinion significant research activity is necessary before we accept/discard the effect of exposed fluorine atoms regarding gas adsorption. The Co^{2+} show dominantly antiferromagnetic coupling followed by the appearance of short-range interaction at low temperature in the case of Co-H*F*MOF-D which could be due to the shorter inter Co^{2+} ion distances compared to those of Co-H*F*MOF-W. Likewise, Mn-H*F*MOF-D shows a dominantly antiferromagnetic nature whereas Mn-H*F*MOF-W shows a paramagnetic nature in the whole measured temperature range. We are continuing to utilize the other neutral bridging coligands along with H_2hfbba to design the new H*F*-MOFs with specific structures and properties.

ASSOCIATED CONTENT

Supporting Information. Description of experimental details, including synthetic methods, crystallography, supplementary figures, including TGA, infrared spectroscopy, PXRD profiles, tables of crystallographic data, CIF files, and anisotropic thermal ellipsoids for H*F*-MOFs reported in this paper. This material is available free of charge via the Internet at http://pubs.acs.org.

AUTHOR INFORMATION

Corresponding Author

*E-mail: r.banerjee@ncl.res.in. Fax: + 91-20-25902636. Phone: + 91-20-25902535.

ACKNOWLEDGMENT

P.P. acknowledges CSIR for a project assistantship (PA-II) from CSIR's XIth Five Year Plan Project (NWP0022-H). R.B. acknowledges Dr. S. Sivaram, Director NCL, for in-house project (MLP020626) and CSIR's XIth Five Year Plan Project (Grant NWP0022-H) funding, and also Dr. B. D. Kulkarni, Dr. S. Pal, and Dr. K. Vijaymohanan for their encouragement. Financial assistance from the DST (SR/S1/IC-22/2009) & (SR/S5/NM-104/2006) is acknowledged.

REFERENCES

(1) (a) Yaghi, O. M.; O'Keeffe, M.; Ockwig, N. W.; Chae, H. K.; Eddaoudi, M.; Kim, J. *Nature* **2003**, *423*, 705. (b) Janiak, C. *J. Chem. Soc., Dalton Trans.* **2003**, 2781. (c) Moulton, B.; Zaworotko, M. J. *Chem. Rev.* **2001**, *101*, 1629. (d) Eddaoudi, M.; Moler, D. B.; Li, H.; Chen, B.; Reineke, T. M.; O'Keeffe, M.; Yaghi, O. M. *Acc. Chem. Res.* **2001**, *34*, 319. (e) Robson, R. *J. Chem. Soc., Dalton Trans.* **2000**, 3735. (f) Yaghi, O. M. *Nat. Mater.* **2007**, *6*, 92. (g) Mueller, U.; Schubert, M.; Teich, F.; Puetter, H.; Schierle-Arndt, K.; Pastre, J. *J. Mater. Chem.* **2006**, *16*, 626. (h) Georgiev, I. G.; MacGillivray, L. R. *Chem. Soc. Rev.* **2007**, *36*, 1239. (i) Corma, A.; Garcia, H.; Xamena, F. X. L. *Chem. Rev.* **2010**, *110*, 4606. (j) James, S. L. *Chem. Soc. Rev.* **2003**, *32*, 276. (k) Yaghi, O. M.; Li, H.; Davis, C.; Richardson, D.; Groy, T. L. *Acc. Chem. Res.* **1998**, *31*, 474. (l) Janiak, C. *Angew. Chem., Int. Ed. Engl.* **1997**, *36*, 1431. (m) Blake, A. J.; Champness, N. R.; Hubberstey, P.; Li, W.-S.; Withersby, M. A.; Schroder, M. *Coord. Chem. Rev.* **1999**, *183*, 117. (n) Murray, L. J.; Dinca, M.; Long, J. R. *Chem. Soc. Rev.* **2009**, *38*, 1294. (o) Kesanli, B.; Cui, Y.; Smith, M.; Bittner, E.; Bockrath, B.; Lin, W. *Angew. Chem., Int. Ed.* **2005**, *44*, 72. (p) Chen, B.; Xiang, S.; Qian, G. *Acc. Chem. Res.* **2010**, *43*, 1115.

(2) (a) Chen, B.; Liang, C.; Yang, J.; Contreras, D. S.; Clancy, Y. L.; Lobkovsky, E. B.; Yaghi, O. M.; Dai, S. *Angew. Chem., Int. Ed.* **2006**, *45*, 1390. (b) Choi, H. J.; Suh, M. P. *J. Am. Chem. Soc.* **2004**, *126*, 15844. (c) Pan, L.; Olson, D. H.; Ciemnolonski, L. R.; Heddy, R.; Li, J. *Angew. Chem., Int. Ed.* **2006**, *45*, 616. (d) Eddaoudi, M.; Kim, J.; Rosi, N.; Vodak, D.; Wachter, J.; O'Keeffe, M..; Yaghi, O. M. *Science* **2002**, *295*, 469. (e) Bourrelly, S.; Llewellyn, P.; Serre, C.; Millange, F.; Loiseau, T.; Ferey, G. *J. Am. Chem. Soc.* **2005**, *127*, 13519. (f) Panella, B.; Hirscher, M.; Puetter, H.; Mueller, U. *Adv. Funct. Mater.* **2006**, *16*, 520. (g) Liu, Y.; Eubank, J. F.; Cairns, A. J.; Eckert, J.; Kravtsov, V. C.; Luebke, R.; Eddaoudi, M. *Angew. Chem., Int. Ed.* **2007**, *46*, 3278.

(3) (a) Caskey, S. R.; Wong-Foy, A. G.; Matzger, A. J. *J. Am. Chem. Soc.* **2008**, *130*, 10870. (b) Millward, A. R.; Yaghi, O. M. *J. Am. Chem. Soc.* **2005**, *127*, 17998. (c) Morris, R. E.; Wheatley, P. S. *Angew. Chem., Int. Ed.* **2008**, *47*, 4966. (d) Kumar, D.-K.; Das, A.; Dastidar, P. *Cryst. Growth Des.* **2007**, *7*, 205. (e) Hu, S.; Zhang, J.-P.; Li, H.-X.; Tong, M.-L.; Chen, X.-M.; Kitagawa, S. *Cryst. Growth Des.* **2007**, *7*, 2286. (f) Chen, B.-L.; Ma, S.-Q.; Zapata, F.; Fronczek, F.-R.; Lobkocsky, E.-B.; Zhou, H.-C. *Inorg. Chem.* **2007**, *46*, 1233. (g) Kitagawa, S.; Kitaura, R.; Noro, S. *Angew. Chem., Int. Ed.* **2004**, *43*, 2334. (h) Thallapally, P. K.; Tian, J.; Motkuri,

R. K.; Fernandez, C. A.; Dalgarno, S. J.; McGrail, P. B.; Warren, J. E.; Atwood, J. L. *J. Am. Chem. Soc.* **2008**, *130*, 16842. (i) Mckinlay, R. M.; Thallapally, P. K.; Atwood, J. L. *Chem. Commun.* **2006**, 2956. (j) Luo, J.; Xu, H.; Liu, Y.; Zhao, Y.; Daemen, L. L.; Brown, C.; Timofeeva, T. V.; Ma, S.; Zhou, H.-C. *J. Am. Chem. Soc.* **2008**, *130*, 9626.

(4) (a) Deshpande, R. K.; Minnaar, J. L.; Telfer, S. G. *Angew. Chem., Int. Ed.* **2010**, *49*, 4598. (b) Wu, C. D.; Hu, A.; Zhang, L.; Lin, W. B. *J. Am. Chem. Soc.* **2005**, *127*, 8940. (c) Shultz, A. M.; Farha, O. K.; Hupp, J. T.; Nguyen, S. T. *J. Am. Chem. Soc.* **2009**, *131*, 4204. (d) Alkordi, M. H.; Liu, Y. L.; Larsen, R. W.; Eubank, J. F.; Eddaoudi, M. *J. Am. Chem. Soc.* **2008**, *130*, 12639. (e) Horike, S.; Dinca, M.; Tamaki, K.; Long, J. R. *J. Am. Chem. Soc.* **2008**, *130*, 5854. (f) Lin, W. B. *J. Solid State Chem.* **2005**, *178*, 2486. (g) Fujita, M.; Kwon, Y. J.; Washizu, S.; Ogura, K. *J. Am. Chem. Soc.* **1994**, *116*, 1151. (h) Seo, J. S.; Whang, D.; Lee, H.; Jun, S. I.; Oh, J.; Jeon, Y. J.; Kim, K. *Nature* **2000**, *404*, 982.

(5) (a) McKinlay, A. C.; Morris, R. E.; Horcajada, P.; Ferey, G.; Gref, R.; Couvreur, P.; Serre, C. *Angew. Chem., Int. Ed.* **2010**, *49*, 2. (b) Rieter, W. J.; Pott, K. M.; Taylor, K. M. L.; Lin, W. *J. Am. Chem. Soc.* **2008**, *130*, 11584. (c) Rieter, W. J.; Taylor, K. M. L.; An, H.; Lin, W. *J. Am. Chem. Soc.* **2006**, *128*, 9024. (d) Horcajada, P.; Serre, C.; Maurin, G.; Ramsahye, N. A.; Balas, F.; Vallet-Regi, M.; Sebban, M..; Taulelle, F.; Ferey, G. *J. Am. Chem. Soc.* **2008**, *130*, 6774. (e) Freiberg, S.; Zhu, X. X. *Int. J. Pharmacol.* **2004**, *282*, 1. (f) Soppimath, K. S.; Aminabhavi, T. M.; Kulkarni, A. R.; Rudzinski, W. E. *J. Controlled Release* **2001**, *70*, 1.

(6) (a) Fang, Q. R.; Zhu, G. S.; Jin, Z.; Ji, Y. Y.; Ye, Y. W.; Xue, M.; Yang, H.; Wang, Y.; Qiu, S.-L. *Angew. Chem., Int. Ed.* **2007**, *46*, 6638. (b) Rosi, N. L.; Eckert, J.; Eddaoudi, M.; Vodak, D. T.; Kim, J.; O'Keeffe, M.; Yaghi, O. M. *Science* **2003**, *300*, 1127. (c) Ma, S. Q.; Sun, D. F.; Simmons, J. M.; Collier, C. D.; Yuan, D. Q.; Zhou, H. C. *J. Am. Chem. Soc.* **2008**, *130*, 1012. (d) Furukawa, H.; Yaghi, O. M. *J. Am. Chem. Soc.* **2009**, *25*, 8876. (e) Furukawa, H.; Kim, J.; Ockwig, N. W.; O'Keeffe, M.; Yaghi, O. M. *J. Am. Chem. Soc.* **2008**, *130*, 11650. (f) Kaye, S. S.; Dailly, A.; Yaghi, O. M.; Long, J. R. *J. Am. Chem. Soc.* **2007**, *129*, 14176. (g) Furukawa, H.; Miller, M. A.; Yaghi, O. M. *J. Mater. Chem.* **2007**, *17*, 3197. (h) Hayashi, H.; Cote, A. P.; Furukawa, H.; O'Keeffe, M.; Yaghi, O. M. *Nat. Mater.* **2007**, *6*, 501. (i) Wong-Foy, A. G.; Matzger, A. J.; Yaghi, O. M. *J. Am. Chem. Soc.* **2006**, *128*, 3494. (j) Choi, H. J.; Dinca, M.; Long, J. R. *J. Am. Chem. Soc.* **2008**, *130*, 7848. (k) Dinca, M.; Long, J. R. *Angew. Chem., Int. Ed.* **2008**, *47*, 6766.

(7) (a) Nakagawa, K.; Tanaka, D.; Horike, S.; Shimomura, S.; Higuchia, M.; Kitagawa, S. *Chem. Commun.* **2010**, *46*, 4258. (b) Wang, B.; Cote, A. P.; Furukawa, H.; O'Keeffe, M.; Yaghi, O. M. *Nature* **2008**, *453*, 207. (c) Walton, K. S.; Millward, A. R.; Dubbeldam, D.; Fros, H.; Low, J. J.; Yaghi, O. M.; Snurr, R. Q. *J. Am. Chem. Soc.* **2008**, *130*, 406. (d) Llewellyn, P. L.; Bourrelly, S.; Serre, C.; Vimont, A.; Daturi, M.; Hamon, L.; Weireld, G. D.; Chang, J.-S.; Hong, D.-Y.; Hwang, Y. K.; Jhung, S. H.; Ferey, G. *Langmuir* **2008**, *24*, 7245. (e) Yazaydn, A. O.; Snurr, R. Q.; Park, T.-H.; Koh, K.; Liu, J.; LeVan, M. D.; Benin, A. I.; Jakubczak, P.; Lanuza, M.; Galloway, D. B.; Low, J. J.; Willis, R. R. *J. Am. Chem. Soc.* **2009**, *131*, 18198. (f) Chandler, B. D.; Cramb, D. T.; Shimizu, G. K. H. *J. Am. Chem. Soc.* **2006**, *128*, 10403. (g) Banerjee, R.; Phan, A.; Wang, B.; Knobler, C.; Furukawa, H.; O'Keeffe, M.; Yaghi, O. M. *Science* **2008**, *319*, 939. (h) Banerjee, R.; Furukawa, H.; Britt, D.; Knobler, C.; O'Keeffe, M.; Yaghi, O. M. *J. Am. Chem. Soc.* **2009**, *131*, 3875.

(8) (a) Blomqvist, A.; Araujo, C. M.; Srepusharawoot, P.; Ahuja, R. *PNAS.* **2007**, *104*, 20173. (b) Li, Z.; Zhu, G.; Lu, G.; Qiu, S.; Yao, X. *J. Am. Chem. Soc.* **2010**, *132*, 1490. (c) Dinca, M.; Dailly, A.; Liu, Y.; Brown, C. M.; Neumann, D. A.; Long, J. R. *J. Am. Chem. Soc.* **2006**, *128*, 16876. (d) Choi, H. J.; Dinca, M.; Dailly, A.; Long, J. R. *Energy Environ. Sci.* **2010**, *3*, 117. (e) Sumida, K.; Horike, S.; Kaye, S. S.; Herm, Z. R.; Queen, W. L.; Brown, C. M.; Grandjean, F.; Long, G. J.; Dailly, A.; Long, J. R. *Chem. Sci.* **2010**, *1*, 184. (f) Dinca, M.; Dailly, A.; Tsay, C.; Long, J. R. *Inorg. Chem.* **2008**, *47*, 11. (g) Roswell, J. L. C.; Yaghi, O. M. *J. Am. Chem. Soc.* **2006**, *128*, 1304. (h) Roswell, J. L. C.; Yaghi, O. M. *Angew. Chem., Int. Ed.* **2005**, *44*, 4670.

(9) (a) Yang, C.; Wang, X.; Omary, M. A. *J. Am. Chem. Soc.* **2007**, *129*, 15454. (b) Yang, C.; Wang, X. P.; Omary, M. A. *Angew. Chem., Int. Ed.* **2009**, *48*, 2500.

(10) Fischer, R. A.; Woll, C. *Angew. Chem., Int. Ed.* **2008**, *47*, 8164.

(11) (a) Hulvey, Z.; Falcao, E. H. L.; Eckert, J.; Cheetham, A. K. *J. Mater. Chem.* **2009**, *19*, 4307. (b) Hulvey, Z.; Sava, D. A.; Eckert, J.; Cheetham, A. K. *Inorg. Chem.* 2011, *50* (2), 403. (c) Pan, L.; Sander, M. B.; Huang, X.; Li, J.; Smith, M.; Bittner, E.; Bockrath, B.; Johnson, J. K. *J. Am. Chem. Soc.* **2004**, *126*, 1308. (d) Yang, W.; Lin, X.; Blake, A. J.; Wilson, C.; Hubberstey, P.; Champness, N. R.; Schroder, M. *Inorg. Chem.* **2009**, *48*, 11067. (e) Fernandez, C. A.; Thallapally, P. K.; Motkuri, R. K.; Nune, S. K.; Sumrak, J. C.; Tian, J.; Liu, J. *Cryst. Growth Des.* **2010**, *10*, 1037. (f) Chun, H.; Dybtsev, D. N.; Kim, H.; Kim., K. *Chem.—Eur. J.* **2005**, *11*, 3521.

(12) (a) Pachfule, P.; Dey, C.; Panda, T.; Vanka, K.; Banerjee, R. *Cryst. Growth Des.* **2010**, *10*, 1351. (b) Pachfule, P.; Dey, C.; Panda, T.; Banerjee, R. *CrystEngComm* **2010**, *12*, 1600.

(13) (a) Robson, R.; Abrahams, B. F.; Batten, S. R.; Gable, R. W.; Hoskins, B. F.; Liu, J. *Supramolecular Architecture*; ACS Publications: Washington, DC, 1992. (b) Hennigar, T. L.; MacQuarrie, D. C.; Losier, P.; Rogers, R. D.; Zaworotko, M. J. *Angew. Chem., Int. Ed. Engl.* **1997**, *36*, 972. (c) Tong, M.-L.; Ye, B.-H.; Cai, J.-W.; Chen, X.-M.; Ng, S. W. *Inorg. Chem.* **1998**, *37*, 2645. (d) Su, C.-Y.; Cai, Y.-P.; Chen, C.-L.; Smith, M. D.; Kaim, W.; Zur Loye, H.-C. *J. Am. Chem. Soc.* **2003**, *125*, 8595. (e) Meng, X.; Song, Y.; Hou, H.; Han, H.; Xiao, B.; Fan, Y.; Zhu, Y. *Inorg. Chem.* **2004**, *43*, 3528. (f) Du, M.; Bu, X.-H.; Guo, Y.-M.; Liu, H.; Batten, S. R.; Ribas, J.; Mak, T. C. W. *Inorg. Chem.* **2002**, *41*, 4904.

(14) (a) Burrows, A. D.; Cassar, K.; Friend, R. M. W.; Mahon, M. F.; Rigby, S. P.; Warren, J. E. *CrystEngComm* **2005**, *7*, 548. (b) Chesman, A. S. R.; Turner, D. R.; Deacon, G. B.; Batten, S. R. *Chem. Commun.* **2010**, *46*, 4899. (c) He, H.; Collins, D.; Dai, F.; Zhao, X.; Zhang, G.; Ma, H.; Sun, D. *Cryst. Growth Des.* **2010**, *10*, 895.

(15) It should be noted that the fluorination referred to in the rest of the article is only partial, as not all the hydrogens were substituted with fluorines in the obtained crystal structures. Reference related to per-fluorinated Metal Organic Framework (*F*-MOFs) has been provided in reference 9a and 9b. Since we have reported only partially fluorinated MOFs here, addition of an "H" to the acronyms has been done to reduce the confusion.

(16) *SMART*, Version 5.05; Bruker AXS, Inc.: Madison, WI, 1998.

(17) *SAINT-Plus*, Version 7.03; Bruker AXS Inc.: Madison, WI, 2004.

(18) Sheldrick, G. M. *SADABS*, Version 2.03, and *TWINABS*, Version 1.02; University of Göttingen: Göttingen, Germany, 2002.

(19) Sheldrick, G. M. *SHELXS '97*; University of Göttingen: Göttingen, Germany, 1997.

(20) Sheldrick, G. M. *SHELXTL '97*; University of Göttingen: Göttingen, Germany, 1997.

(21) Spek, A. L. *PLATON, A Multipurpose Crystallographic Tool*; Utrecht University: Utrecht, The Netherlands, 2005.

(22) The abbreviation −D and −W corresponds to H_2O and DMF respectively.

(23) Addison, A. W.; Rao, T. N.; Reedijk, J.; Rijn, J. V.; Verschoor, G. C. *J. Chem. Soc., Dalton Trans.* **1984**, 1349.

(24) (a) O'Keefe, M.; Eddaoudi, M.; Li, H.; Reineke, T. M.; Yaghi, O. M. *J. Solid State Chem.* **2000**, *152*, 3. (b) Tranchemontagne, D. J.; Mendoza-Cortes, J. L.; O'Keefe, M.; Yaghi, O. M. *Chem. Soc. Rev.* **2009**, *38*, 1257. (c) Mellot-Draznieks, C.; Dutour, J.; Ferey, G. *Angew. Chem., Int. Ed.* **2004**, *43*, 6290.

(25) *All calculation were done using Cerius*^{2} software (Ver. 4.2, Accelrys); van der Waals radii were taken into consideration in all cases (C, 1.70; H, 1.20; O, 1.52; N, 1.55; Cl, 1.79; Br, 1.89 Å).

(26) (a) Golovanov, D. G.; Lyssenko, K. A.; Antipin, M. Y.; Vygodskii, Y. S.; Lozinskaya, E. I.; Shaplov, A. S. *CrystEngComm* **2005**, *7*, 53. (b) Althoff, G.; Ruiz, G.; Rodríguez, V.; López, G.; Pérez, J.; Janiak, C. *CrystEngComm* **2006**, *8*, 662. (c) Takahashi, S.; Jukurogi, T.; Katagiri, T.; Uneyama, K. *CrystEngComm* **2006**, *8*, 320. (d) Choudhury, A. R.; Guru Row, T. N. *CrystEngComm* **2006**, *8*, 265. (e) Mariaca, R.; Behrnd, N.-R.; Eggli, P.; Stoeckli-Evans, H.; Hulliger, J. *CrystEngComm* **2006**, *8*, 222. (f) D'Oria, E.; Novoa, J. J. *CrystEngComm* **2008**, *10*, 423. (g) Desiraju, G. R.; Steiner, T. In *IUCr Monograph on Crystallography*;

Oxford Science: Oxford, 1999; Vol. 9. (h) Ruiz, J.; Rodríguez, V.; Haro, C. D.; Espinosa, E.; Pérez, J.; Janiak, C. *Dalton Trans.* **2010**, *39*, 3290.
(27) (a) Flack, H. D.; Bernardinelli, G. *Acta Crystallogr.* **1999**, *A55*, 908. (b) Flack, H. D. *Acta Crystallogr.* **1983**, *A39*, 876.
(28) (a) Janiak, C.; Chamayou, A.-C.; Royhan Uddin, A. K. M.; Uddin, M.; Hagen, K. S.; Enamullah, M. *Dalton Trans.* **2009**, 3698. (b) Gil-Hernandez, B.; Gili, P.; Vieth, J. K.; Janiak, C.; Sanchiz, J. *Inorg. Chem.* **2010**, *49*, 7478.
(29) Li, J.-R.; Kuppler, R. J.; Zhou, H.-C. *Chem. Soc. Rev.* **2009**, *38*, 1477.
(30) (a) Zhao, X.; Xiao, B.; Fletcher, A. J.; Thomas, K. M. *J. Phys. Chem. B.* **2005**, *109*, 8880. (b) Sircar, S.; Golden, T. C.; Rao, M. B. *Carbon* **1996**, *34*, 1.
(31) Ouellette, W.; Prosvirin, A. V.; Valeioh, J.; Dunbar, K. R.; Zubieta, J. *Inorg. Chem.* **2007**, *46*, 9067.
(32) Daniel, C.; Hart, H. *J. Am. Chem. Soc.* **2009**, *131*, 5101.